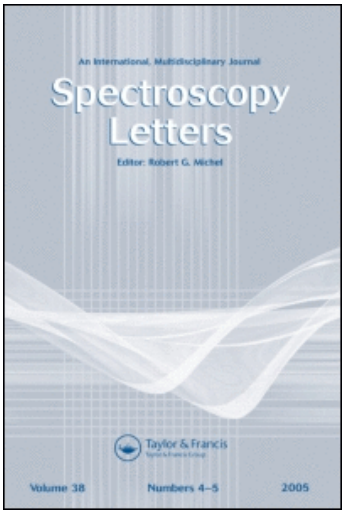

Spectroscopy Letters
Publication details, including instructions for authors and subscription information:
http://www.informaworld.com/smpp/title~content=t713597299

Spectroscopic Application of Realgar Using X-ray Fluorescence and Raman Spectroscopy

Yusuf Kağan Kadıoğlu[a]; Zafer Üstündağ[b]; Zafer Yazıcıgil[c]
[a] Geological Engineering Department, Faculty of Engineering, Ankara University, Ankara, Turkey [b] Chemistry Department, Faculty of Art & Science, Dumlupinar University, Kütahya, Turkey [c] Chemistry Department, Faculty of Art & Science, Selçuk University, Konya, Turkey

To cite this Article Kadıoğlu, Yusuf Kağan , Üstündağ, Zafer and Yazıcıgil, Zafer(2009) 'Spectroscopic Application of Realgar Using X-ray Fluorescence and Raman Spectroscopy', Spectroscopy Letters, 42: 3, 121 — 128
To link to this Article: DOI: 10.1080/00387010902728825
URL: http://dx.doi.org/10.1080/00387010902728825

Spectroscopy Letters, 42:121–128, 2009

ISSN: 0038-7010 print/1532-2289 online
DOI: 10.1080/00387010902728825

Taylor & Francis
Taylor & Francis Group

Spectroscopic Application of Realgar Using X-ray Fluorescence and Raman Spectroscopy

Yusuf Kağan Kadıoğlu[1], Zafer Üstündağ[2], and Zafer Yazıcıgil[3]

[1]Faculty of Engineering, Ankara University, Geological Engineering Department, Ankara, Turkey
[2]Faculty of Art & Science, Dumlupinar University, Chemistry Department, Kütahya, Turkey
[3]Faculty of Art & Science, Selçuk University, Chemistry Department, Konya, Turkey

ABSTRACT Samples of realgar ore were collected from the hydrothermal products of the Eocene volcanic material of the Erzurum region in Turkey. The prepared samples were analyzed by polarized energy dispersive X-ray fluorescence (PEDXRF) and by confocal Raman spectroscopy (CRS). The goal of this study was to figure out the chemical composition of realgar and its properties through PEDXRF and CRS and the optical characteristic features under the polarized microscope. The result of the XRF analysis shows the collected realgar samples are mainly composed of As, S, Si, and Mg in different proportions. The contents of As in realgar change from 36.55% through 31.49% to 5.97% in the analyzed samples. The strong peak of the realgar samples is at 352 cm^{-1}, and a weaker peak exists around 190 cm^{-1}. The accuracy and precision of the technique for chemical analysis is demonstrated by analyzing CRM 2126-81. The realgar ores were studied by use of CRS and polarized microscopy.

KEYWORDS Raman, realgar, X-ray fluorescence

INTRODUCTION

Realgar (AsS) is crystallized in a monoclinic system as prismatic crystals and generally is coarse to fine granular size. This mineral has ring-like structure groups of As_4S_4. Due to hydrothermal alterations, some parts of realgar (AsS) may alter to pararealgar (As_4S_4) forming a light-yellow color. It is very soft with 1.5–2 hardness and has a gravity of 3.4 g/cm^3. Realgar is streaked red to orange in color and may associate with the yellowish orpiment (As_2S_3). It may also accompany arsenopyrite, sphalerite, antimonite, arsenic-sulfosalts, and pyrite. It is softer than orpiment and antimonite. Realgar is very striking in hand and has small grain sizes with high internal reflection under the microscope. It occurs in veins of lead, silver, and gold-associated hydrothermal deposits. Realgar may be used in fireworks for giving a brilliant white light and also used for artificial arsenic sulfide.

In past years, rapid and nondestructive analyses have became important in analytical techniques. However, the XRF technique has several advantages for chemical and geochemical analysis.[1,2]

Received 23 April 2008; accepted 1 September 2008.

Address correspondence to Yusuf Kağan Kadıoğlu, Ankara University, Faculty of Engineering, Geological Engineering Department, Ankara, Turkey. E-mail: kadi@eng.ankara.edu.tr

Marguí et al. studied the multielemental fast analysis of vegetation samples by XRF spectroscopy.[3] They reported that the XRF technique was a universally nondestructive method for rapid and sequential or simultaneous quantitative analysis of materials. Bichinho and co-workers determined the catalyst metal residues in polymer samples by XRF.[4] They reported that XRF could provide an element analysis in the polymer matrix through a direct analysis in $\mu g\ kg^{-1}$ levels.

Camerani and co-workers studied the XRF tomography of individual municipal solid waste (MSW) and biomass fly ash particles.[5] They reported that the technique was able, for the first time, to show the internal concentration distribution of macro and micro elements in the microscopic and highly inhomogeneous objects, like particles of fly ash, with very little sample preparation requirements. Goldstein et al. characterized a soil by energy dispersive X-ray fluorescence (EDXRF) spectroscopy in an environmental study.[1] They searched from K to U as elements in their study. Siyanbola et al. analyzed zircon samples of Nigeria by the ED-XRF,[6] searching 22 elements in the zircon samples, and compared two types of zircon samples. Perring and co-workers performed an elemental analysis of infant cereal samples by wavelength dispersive XRF spectroscopy.[7] This study involved investigating 88 samples of commercially available products. They analyzed 9 elements (Na, Mg, P, Cl, K, Ca, Mn, Fe, and Zn). Vantelon and co-workers investigated the spatial distribution and speciation of Pb in the weathering crust and soil surrounding corroding metallic lead bullets in a shooting-range soil.[8] They analyzed the soil samples by the micro-XRF technique.

There are many investigations regarding the nature and behavior of the elements in river water, surface sediments of rivers,[9,10] soil samples,[11–13] geological samples,[14] aerosols in urban enviroment,[15] in various vegetables,[16–19] and in blood and biological samples.[20,21]

As a result, the XRF technique, especially the EDXRF technique, is one of the most popular methods for quantitative analysis and is a highly recommended technique.[2]

Raman spectroscopy is an important analytical technique. It provides information about the composition of composites, pigments, semiconductor materials, biological structures, polymers,[22] and geological samples.[23–28] Üstündağ and co-workers characterized trona mineral by confocal Raman spectroscopy. They reported that the identification of the trona was controlled by Raman confocal spectroscopy.[23] Recent studies show that confocal Raman spectroscopy is a useful analysis technique for determination in mineral science.[29–36]

Blach et al. explained the geometry of the Raman spectra as a collected data set of spectra in a confocal polarized micro-Raman and back-scattered geometry. They reported that the analyzed material could be either rotated around the optical axis of the microscope through which the pump was focused onto the sample or vertically translated, as depicted.[37]

The focus of the current study is to investigate the geochemical compositions and behavior of the element distribution of realgar and its all rock using polarized energy dispersive X-ray fluorescence (PEDXRF), conform Raman spectroscopy (CRS), and optical characteristics under polarized microscopy.

Geological Features of Realgar

The realgar of the Eocene volcanic region of Erzurum has a wide exposure along the veins ranging in width from 40 cm up to 15 m. The volcanic material of this area is mainly composed of augite basalt and augite–hornblende andesite. The realgar of Erzurum occurs in a different part of the eastern Anatolian volcanic province as a cluster and powder products at the surface of the outcrops. It has gradual contact with the host rock and may also be observed as disseminated products along the contact within the wall rocks. The collected samples represent the pure ore (S1), powder samples (S2), and the disseminated samples within the wall rock (S3) (Table 1).

Optical Features under the Polarized Microscope

The realgar samples were sliced and polished to about 0.03 mm thick for the optical mineralogy and

TABLE 1 Codes for the Samples

Sample	Code
Realgar, crystal (pure)	S1
Realgar, powder	S2
Realgar, wall rock	S3

polarized microscopy (Leica Microsystems, Wetzlar, Germany) studies. In this method, a chip is cut out and the surface of the samples is polished and glued by Canada balsam to the slide glass. The upper surface of the sample was polished using progressively finer and finer abrasive.[38] The sample was ground down to its final thickness of about 0.03 mm. Realgar polishes poorly due to its low hardness. Polishing cleavage is hardly observed and it has bright luster and gray-white reflection under polarized microscopy. The realgar has yellow-red with immersion present everywhere as internal reflection under the polarizing microscope. It can be distinguished from other minerals by its low hardness, orange–red streak and red color with small grains, and its typical internal reflection.

METERIALS AND METHODS

Sample Preparation for PEDXRF Measurement

The samples used in this study were gathered from Erzurum in Turkey according to the sampling methods. All samples were ground into fine powder in an agate mortar. They were sieved to pass through a 200-μm mesh and then pressed into thick pellets of 32 mm diameter using wax (Breitländer GmbH, Hamm, Germany) as binder. CRM 2126-81 (Asso, France) was equally pressed into pellets in a similar manner as the samples, and these were used for quality assurance.[11,23,39,40]

Multielement concentration was determined by using PED-XRF. The spectrometer used in this study was a Spectro XLAB 2000 PEDXRF spectrometer (Germany), which was equipped with a Rh anode X-ray tube, 0.5 mm Be side window. The detector of the spectrometer is Si(Li) by liquid N_2 cooled with resolution of <150 eV at Mn Kα, 5000 cps. The PEDXRF spectrometer configures source beam, scattered beam, and fluorescent beam in all at mutually orthogonal angles.[41]

The sample is measured by PEDXRF mainly done by three types of targets.[41] The first target is suitable for the light elements with $Z > 22$, and this target is named as Barkla target. The second target is oriented crystal target that is suitable for light elements up to $Z = 22$ and can be named as Bragg target. The third target is pure metal target and is suitable for specific elements or small groups of adjacent elements. In addition, this target is helpful for generating Compton scatter peaks, which can be used for matrix correction.

Confocal Raman Spectrometer Analysis

The realgar samples from the study area were collected according to the sampling methods. The samples were prepared and polished for the analyses under polarized microscopy and Raman confocal micro-spectroscopy. The samples were studied by a HORIBA Jobin Yvon-HR800 confocal Raman Spectrometer (France) for identification of realgar. The confocal Raman spectroscopy (CRS) is a well-known method for the analyses of minerals, however, CRS has not yet been widely applied to realgar identification and determination. Raman measurements were performed with a HORIBA Jobin Yvon spectrometer equipped with a laser operating at a wavelength of 633 nm. An electrical cooled charge-coupled device (CCD) detector was employed to acquire spectra, and the laser spot was focused on realgar surface with 10×, 50×, or 100× long focused objectives, which allow a 65- and 13-mm working distance, respectively, and a lateral resolution of 5 and 2 μm, respectively. Polarization of the incident laser beam was selected parallel to the preferential domain orientation of samples (y), and spectra were collected in a strict backscattering geometry. The intensity values of phonon modes for realgar were obtained using a Labspec 4.02 (HORIBA Jobin Yvon) package, according to the Gaussian–Lorentzian mixed functions after subtracting a baseline and applying the initial approximations of modes position.[23,42]

RESULTS AND DISCUSSION

All data are the result of an average of three measurements on each sample with a relative standard deviation (SD) of generally less than 10%. The concentration values of the 33 elements searched are given in Table 2. Results were calculated by considering the loss on ignition (LOI). Concentrations of elements are given in $\mu g\,g^{-1}$ except for those of major elements, which are given in percent. (Table 2). For illustration, the PEDXRF spectrum of the main elements of the wall rock realgar are given in Fig. 1.

TABLE 2 Multielemental Concentrations (Mean ± SD) in the Realgar samples*

Element	S1	S2	S3
Na	1.86 ± 0.21%	1.08 ± 0.16%	2450 ± 130
Mg	4.00 ± 0.16%	3.24 ± 0.14%	2.768 ± 0.087%
Al	ND	1.539 ± 0.023%	5.12 ± 0.029%
Si	3.461 ± 0.027%	15.90 ± 0.05%	19.97 ± 0.04%
P	597 ± 41	623 ± 36	693 ± 21
S	20.47 ± 0.04%	17.09 ± 0.03%	2.704 ± 0.008%
Cl	43.8 ± 3.2	ND	ND
K	1335 ± 87	5320 ± 120	9039 ± 99
Ca	782 ± 40	2403 ± 60	5.484 ± 0.019%
Ti	454 ± 24	2498 ± 40	4407 ± 39
V	ND	71 ± 15	215 ± 15
Cr	ND	ND	324 ± 17
Mn	71 ± 26	ND	973 ± 24
Fe	1062 ± 33	2.216 ± 0.014%	6.249 ± 0.015%
Ni	230 ± 12	192 ± 12	139.1 ± 5.7
Cu	ND	20.3 ± 7.4	82.2 ± 4.3
Zn	102.3 ± 9.1	107.2 ± 9.3	95.3 ± 3.9
Ga	36.9 ± 5.4	37.5 ± 5.4	21.7 ± 2.1
As	36.55 ± 0.05%	31.49 ± 0.04%	5.974 ± 0.009%
Rb	ND	ND	26.5 ± 1.0
Sr	5.6 ± 1.9	8.8 ± 2.4	260.5 ± 2.3
Y	ND	ND	16.0 ± 1.1
Zr	ND	23.9 ± 6.5	61.1 ± 5.8
Nb	ND	ND	11.9 ± 3.0
Ag	ND	3.5 ± 1.8	ND
Cd	2.9 ± 1.1	ND	ND
Sn	4.0 ± 0.8	3.0 ± 0.7	1.9 ± 0.5
Sb	ND	112.8 ± 2.0	27.0 ± 0.8
Te	ND	ND	1.8 ± 0.9
Ba	13.4 ± 3.0	88.2 ± 3.7	277.8 ± 4.2
Ce	ND	ND	12.2 ± 5.9
Hg	1063 ± 30	846 ± 27	80.9 ± 7.4
U	70 ± 12	21 ± 12	23.9 ± 6.3

*Concentrations of elements are given in $\mu g\,g^{-1}$ except for those of major elements given in percent (%).

TABLE 3 The Content of the Elements Obtained from the Certified Material CRM 2126-81 by using PEDXRF (with 95% confidence) Quantitative Method*

Elements or oxide	Certificate concentration	Measurement concentration
SiO_2	64.45 ± 0.09%	63.71 ± 0.07%
Al_2O_3	16.61 ± 0.13%	15.47 ± 0.04%
MgO	1.58 ± 0.04%	1.44 ± 0.04%
CaO	3.82 ± 0.05%	3.699 ± 0.007%
Na_2O	4.27 ± 0.08%	4.19 ± 0.14%
K_2O	3.12 ± 0.04%	3.502 ± 0.06%
TiO_2	6300 ± 200	5900 ± 200
P_2O_5	2290 ± 100	2076 ± 100
MnO	830 ± 50	974 ± 40
Fe_2O_3	4.64 ± 0.09%	4.48 ± 0.02%
Ba	970 ± 80	876 ± 5
Co	7.6 ± 0.7	7.2 ± 1.3
Cr	21 ± 2	20.2 ± 1.8
Cu	16 ± 2	15.4 ± 0.8
Ga	27 ± 2	26.4 ± 0.6
Ge	1.1 ± 0.2	ND
La	54 ± 7	52.6 ± 2.7
Mo	2.0 ± 0.3	1.98 ± 0.2
Nb	15 ± 3	14.3 ± 1.2
Ni	9.5 ± 0.9	9.4 ± 1.0
Pb	19 ± 2	18.4 ± 0.6
Rb	121 ± 8	120.9 ± 0.4
Sn	4.6 ± 0.5	4.4 ± 0.2
Sr	500 ± 50	491.1 ± 2
V	70 ± 6	65.4 ± 5.4
Y	25 ± 3	22.8 ± 0.3
Zn	69 ± 7	60.8 ± 1.2
Zr	230 ± 20	229.3 ± 1.0

*Concentrations of elements are given in $\mu g\,g^{-1}$ except for those of major elements given in percent (%). Precision is given as standard deviation in each case for three different measurements.

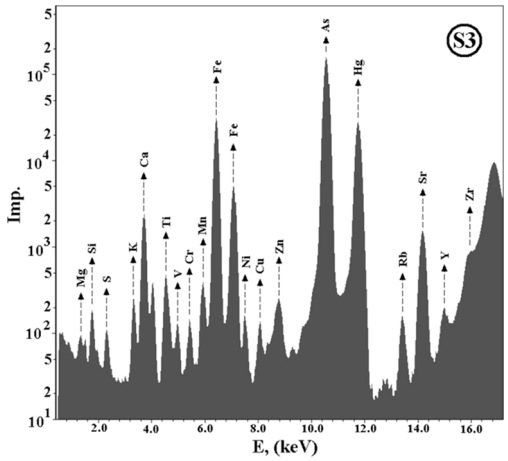

FIGURE 1 XRF spectrum of realgar sample (S3: wall rock).

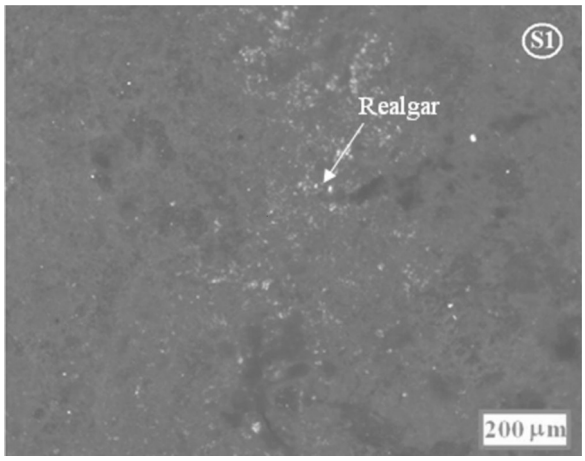

FIGURE 2 Microphotograph of pure realgar sample (S1) under the polarized microscope.

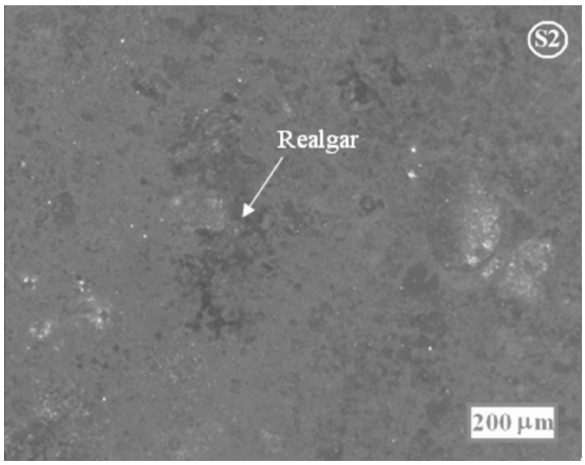

FIGURE 3 Microphotograph of powder realgar sample (S2) under the polarized microscope.

The results of the measurements of the PEDXRF Spectro XLAB 2000 PEDXRF spectrometer (Germany) spectrometer were controlled by determining the elemental concentration in a standard sample prepared with CRM 2126-81 as shown in Table 3.

The results of the geochemical analysis of the realgar samples revealed that the S1, S2, and S3 have 36.55%, 31.49%, and 5.974% of As, respectively. The pure realgar (Fig. 2) sample (S1) has higher concentration of As and Ni than do the powder realgar (Fig. 3) sample (S2) and wall rock (S3) sample (Fig. 4). The wall rock sample has low amount of As, because it has disseminated with limited amount of realgar concentrations. The polarized microscope views of the all samples are shown in Figs. 2, 3, and 4.

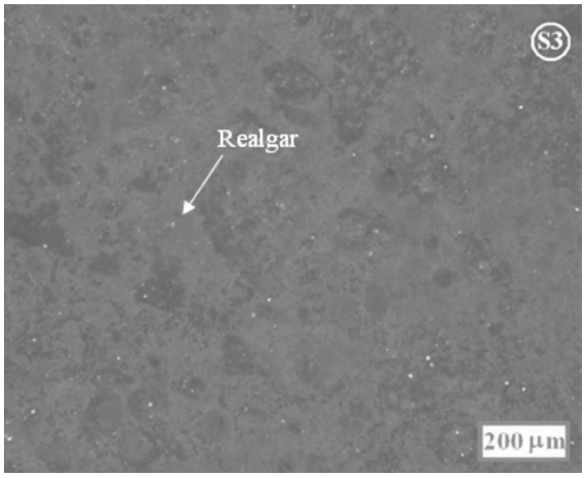

FIGURE 4 Microphotograph of wall rock realgar (pararealgar) sample (S3) under the polarized microscope.

Photomicrographs of the Raman spectra of the realgar samples are given in Figs. 5, 6, and 7. The confocal Raman spectroscopy reveals clear Raman spectra for S1 and S2 samples (Fig. 8). The spectrum

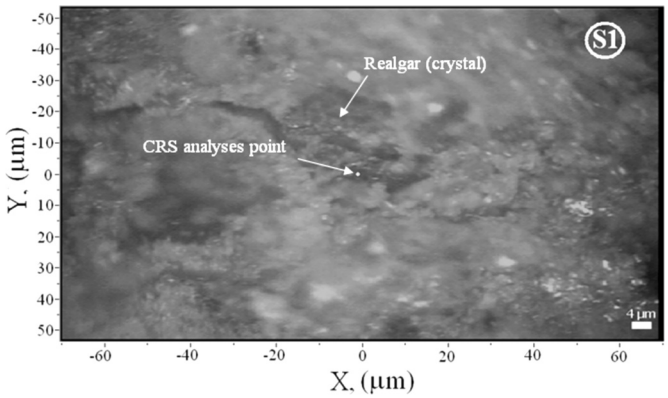

FIGURE 5 Microview of confocal Raman microscope (France) image of pure realgar (S1) and its analysis point.

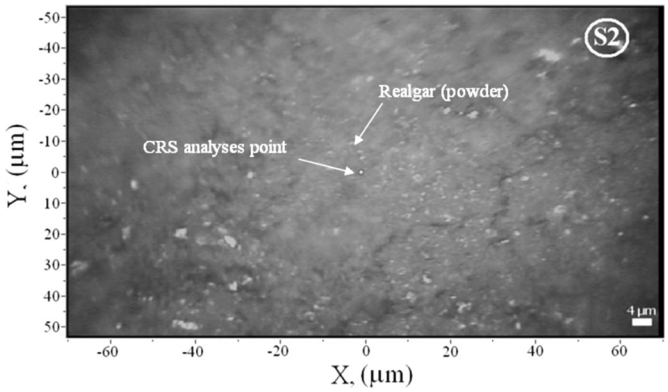

FIGURE 6 Microview of confocal Raman microscope (France) image of powder realgar sample (S2) and its analysis point.

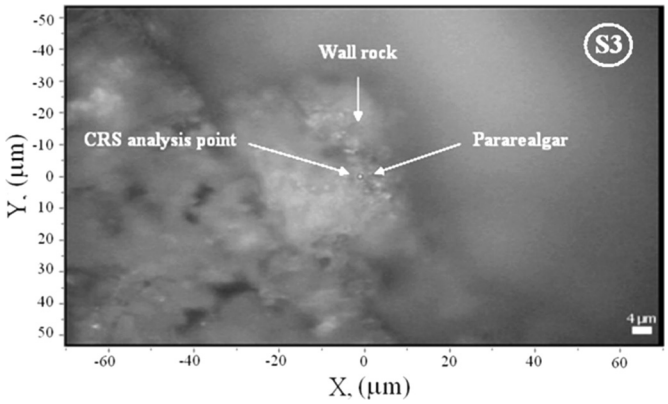

FIGURE 7 Microview of confocal Raman microscope (France) image of wall rock realgar (pararealgar) sample (S3) and its analysis point.

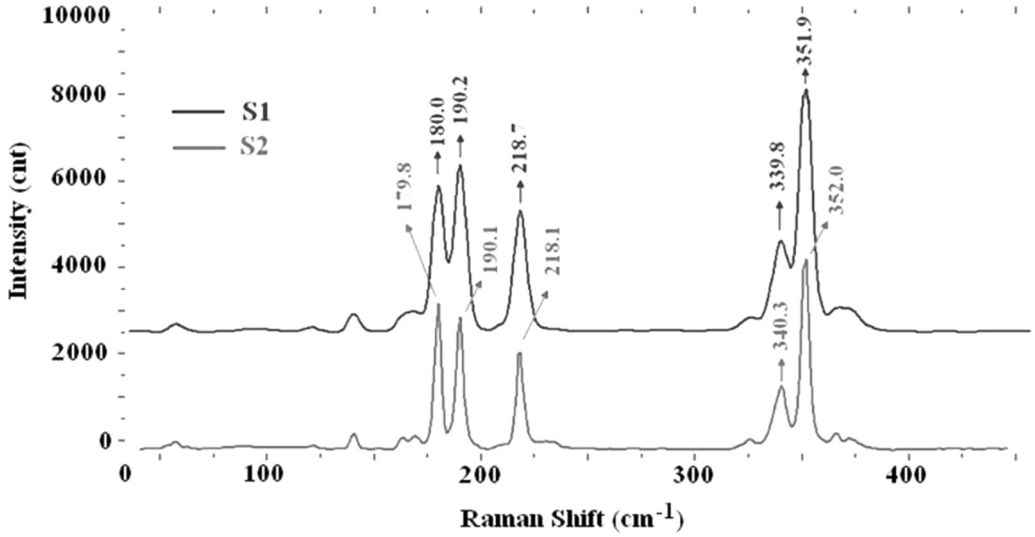

FIGURE 8 Confocal Raman spectrum of pure (S1) and powder (S2) realgar samples.

of S3 (Fig. 9) is not identical with those of the S1 and S2 samples (Fig. 8), but it is most identical with the pararealgar spectra (Fig. 9). Pararealgar is a polymorph of realgar that may form as an interaction of realgar with hydrothermal solution of the residual fluids of the system.

The S1 and S2 are represented the realgar samples with a strong peaks near 352 cm^{-1} and a weaker peak around 190 cm^{-1} (Fig. 8). The strong Raman spectrum peak (around 352 cm^{-1}) of pure realgar is derived from As–S stretching and the weak peaks (around 180.0 cm^{-1}, 190.0 cm^{-1}, and 218.0 cm^{-1}) may derive from As–As stretching +As–S–As bending. The weak peak of 218.7 cm^{-1} for S1 and 218.1 cm^{-1} for S2 in Fig. 8 may be the result of a weak transformation of realgar to polymorph realgar. On the other hand, the Raman spectrum of the wall rock sample is most similar to the Raman spectrum of the polymorph (pararealgar, As_4S_4) spectrum (Fig. 9). The studied sample of S3 has a pair of strong peaks near 228.7 cm^{-1} representing the polymorph structure of realgar, which is a pararealgar. It may be concluded that the appearance of a pair of strong peaks (As–As–S bending) near 228.7 cm^{-1} may differentiate realgar from the pararealgar. The As–As stretching modes and the strong band are around 350 cm^{-1} which represent the totally symmetric vibration of the covalently bonded S–As–S–As

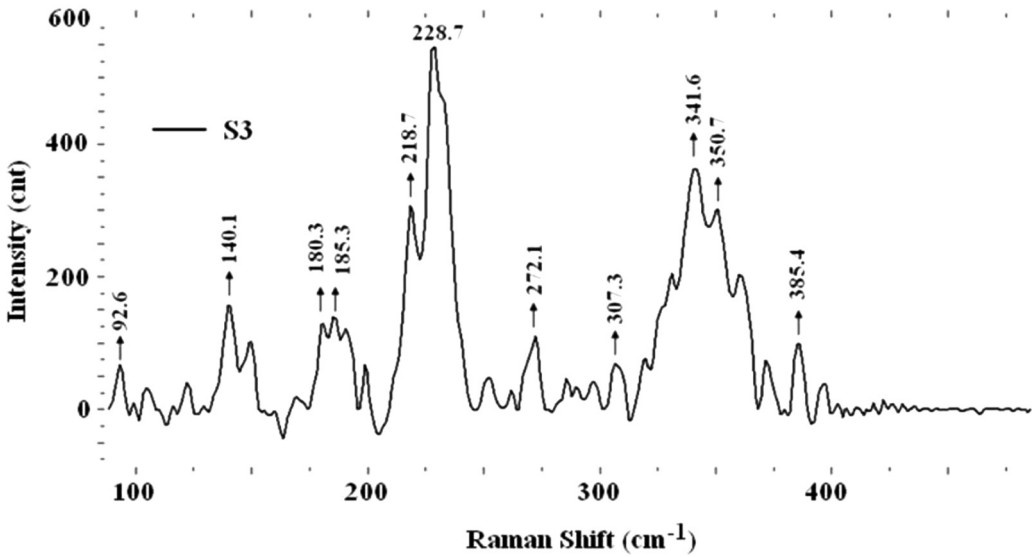

FIGURE 9 Confocal Raman spectrum of wall rock realgar (pararealgar) sample.

chain.[43,44] The Raman spectrum results of S3 reveal that the realgar is transformed to pararealgar during the alteration at the contact of the wall rock. As a result, the pararealgar spectrum (S3) has a greater number of bands of strong or medium ($92.6\,cm^{-1}$, $140.1\,cm^{-1}$, $272.1\,cm^{-1}$, $307.1\,cm^{-1}$, and $385.1\,cm^{-1}$ in Fig. 9) intensity, which may reflect reduced molecular symmetry of pararealgar (S3 in Fig. 9) with respect to realgar (S1 and S2 in Fig. 8).

CONCLUSIONS

The geochemical composition of realgar and its wall rock samples were analyzed by the PEDXRF. The identification of the realgar was performed by polarized microscopy and Raman confocal spectroscopy. The mineralogical and PEDXRF results of realgar reveal that realgar (S1) is more pure than the powder realgar (S2). The realgar at the surface of wall rock has less arsenic content because of the transformation of realgar to the polymorph structure. Moreover, the pure realgar (S1) has a clearer Raman spectrum than that of the powder realgar (S2). The hydrothermal alteration products produce a pair of strong peaks near $228.7\,cm^{-1}$ of As–As–S bending at the contact of wall rock during the hydrothermal alteration. Raman spectroscopy is quite useful during the differentiation of realgar from the pararealgar by the appearance of a pair of strong peaks of As–As–S bending during the transformation. As a conclusion, the PEDXRF technique, Raman confocal spectroscopy, and polarized microscopy are useful methods for quantitative and geochemical studies in determination, behavior during the alteration, and for comparison of minerals in material sciences.

ACKNOWLEDGMENT

The authors would like to thank Ankara University for the supporting the projects DPT 2003-K-120-190-4-6 and BAP 2007-07-45-056.

REFERENCES

1. Goldstein, S. J.; Slemmons, A. K.; Canavan, H. E. Energy-dispersive X-ray fluorescence methods for environmental characterization of soils. *Environ. Sci. Technol.* **1996**, *30*, 2318–2321.
2. Bertin, F. P. *Principles and Practice of X-ray Spectrometric Analysis,* 2nd ed., Plenum Press: New York, 1975.
3. Marguí, E.; Hidalgo, M.; Queralt, I. Multi-elemental fast analysis of vegetation samples by wavelength dispersive X-ray fluorescence spectrometry: Possibilities and drawbacks. *Spectrochim. Acta B* **2005**, *60*, 1363–1372.
4. Bichinho, K.; M. Pozzobon, G.; Stedile, F. C.; dos Santos, J. H. Z.; Wolf, C. R. Determination of catalyst metal residues in polymers by X-ray fluorescence. *Spectrochim Acta B* **2005**, *60*, 599–604.
5. Camerani, M. C.; Golosio, B.; Somogyi, A.; Simionovici, A. S.; Steenari, B. M.; Panas, I. X-ray fluorescence tomography of individual municipal solid waste and biomass fly ash particles. *Anal. Chem.* **2004**, *76*, 1586–1595.
6. Siyanbola, W. O.; Fasasi, A. Y.; Funta, I. I.; Fasasi, M. K.; Tubosun, I. A.; Pelemo, D. A.; Adesiyan, T. A. Energy dispersive X-ray fluorescence analysis of samples of the Nigerian Zircons. *Nucl. Instrum. Methods B* **2005**, *239*, 426–432.
7. Perring, L.; Andrey, D.; Basic-Dvorzak, M.; Blanc, J. Rapid multimineral determination in infant cereal matrices using wavelength dispersive X-ray fluorescence. *Agric. Food Chem.* **2005**, *53*, 4696–4700.
8. Vantelon, D.; Lanzirotti, A.; Scheinost, A. C.; Kretzschmar, R. Spatial distribution and speciation of lead around corroding bullets in a shooting range soil studied by micro-X-ray fluorescence and absorption spectroscopy. *Environ. Sci. Technol.* **2005**, *39*, 4808–4815.
9. Costa, A. C. M.; Castro, C. R. F.; Anjos, M. J.; Lopes, R. T. J. Multielement determination in river-water of Sepetiba Bay tributaries (Brazil) by total reflection X-ray fluorescence using synchrotron radiation. *Radioanal. Nucl. Chem.* **2006**, *269*, 703–706.
10. Pereira, M. O.; Calza, C.; Anjos, M. J.; Lopes, R. T.; Araújo, F. G. J. Metal concentrations in surface sediments of Paraíba do sul River (Brazil). *Radioanal. Nucl. Chem.* **2006**, *269*, 707–709.
11. Üstündağ, Z.; Kalfa, O. M.; Erdoğan, Y.; Kadıoğlu, Y. K. Elemental speciation of different stages of silver metal recovery process using PEDXRF. *Nucl. Instrum. Methods. B* **2006**, *251*, 213–217.
12. Cojocaru, V.; Strumińska, D. I.; Pantelică, A.; Pincovschi, E.; Georgescu, I. I. EDXRF versus INAA in a pollution control of soil. *J. Radioanal. Nucl. Chem.* **2006**, *268*, 71–78.
13. Fabbi, B. P. X-Ray fluorescence determination determination of Barium and Strontium in Geologic samples. *Appl. Spectrosc.* **1971**, *25*, 316–318.
14. Tahboub, Y. R. Determination of major and minor elements in granite by inductively coupled plasma and X-ray fluorescence spectrometry. *Anal. Lett.* **1994**, *27*, 401–410.
15. Boman, J.; Gatari, M. J.; Wagner, A.; Hossain, M. I. Elemental characterization of aerosols in urban and rural locations in Bangladesh. *X-ray Spectrom.* **2005**, *34*, 460–467.
16. Uskoković-Marković, S.; Todorović, M.; Mioć, U. B.; Antunović-Holclajtner, I.; Andrić, V. EDXRF spectrometry determination of tungsten in tobacco plants after antiviral treatment with 12-tungstophosphoric acid and its compounds. *Talanta* **2006**, *70*, 301–306.
17. Oreščanin, V.; Mikelić, L.; Lovrenčić, I.; Barišić, D.; Mikulić, N.; Lulić, S. Environmental contamination assessment of the surroundings of the Ex-Ferrochromium Smelter Dugi Rat, Croatia. *J. Environ. Sci. Heal. A* **2006**, *41*, 2547–2555.
18. de Oliveira, A. L.; de Almeida, E.; da Silva, F. B. R.; Filho, V. F. N. Elemental contents in exotic Brazilian tropical fruits evaluated by energy dispersive X-ray fluorescence. *Sci. Agric.* **2006**, *63*, 82–84.
19. Noda, T.; Tsuda, S.; Mori, M.; Takigawa, S.; Matsuura-Endo, C.; Kim, S.-J.; Hashimoto, N.; Yamauchi, H. Determination of the phosphorus content in potato starch using an energy-dispersive X-ray fluorescence method. *Food Chem.* **2006**, *95*, 632–637.
20. Serpa, R. F. B.; de Jesus, E. F. O.; Anjos, M. J.; Lopes, R. T.; do Carmo, M. G. T.; Rocha, M. S.; Rodrigues, L. C.; Moreira, S.; Martinez, A. M. B. Cognitive impairment related changes in the elemental concentration in the brain of old rat. *Spectrochim. Acta B* **2006**, *61*, 1219–1223.
21. Custódio, P. J.; Carvalho, M. L.; Nunes, F.; Pedroso, S.; Campos, A. J. Direct analysis of human blood (mothers and newborns) by energy

dispersive X-ray fluorescence. *Trace Elem. Med. Biol.* **2005**, *19*, 151–158.
22. Tabaksblat, R.; Meier, R. J.; Kip, B. J. Confocal Raman Microspectroscopy: Theory and application to thin polymer samples. *Appl. Spectrosc.* **1992**, *46*, 60.
23. Üstündağ, İ.; Üstündağ, Z.; Kalfa, O. M.; Kadıoğlu, Y. K. Geochemical compositions of trona samples by PEDXRF and their identification under Confocal Raman Spectroscopy: Beypazari-Ankara, TURKEY. *Nucl. Instrum. Methods B* **2007**, *254*, 153.
24. Bozlee, B. J.; Misra, A. K.; Sharma, S. K.; Ingram, M. Remote Raman and fluorescence studies of mineral samples. *Spectrochim. Acta A* **2005**, *61*, 2342–2348.
25. Spötl, C.; Houseknecht, D. W.; Jaques, R. C. Kerogen maturation and incipient graphitization of hydrocarbon source rocks in the Arkoma Basin, Oklahoma and Arkansas: a combines petrographic and Raman spectrometric study. *Org. Geochem.* **1998**, *28*, 535–542.
26. Yamamoto, J.; Kagi, H.; Kaneoka, I.; Lai, Y.; Prikhod'ko, V. S.; Arai, S. Fossil pressures of fluid inclusions in mantle xenoliths exhibiting rheology of mantle minerals: implications for the geobarometry of mantle minerals using micro-Raman spectroscopy. *Earth Planet Sci. Lett.* **2002**, *198*, 511–519.
27. Rudolph, W. W.; Mason, R. J. Study of Aqueous $Al_2(SO_4)^3$ solution under hydrothermal conditions: Sulfate ion pairing, hydrolysis, and formation of Hydronium Alunite. *Solution Chem.* **2001**, *30*, 527–548.
28. Gucsik, A.; Koeberl, C.; Brandstätter, F.; Reimold, W. U.; Libowitzky, E. *Cathodoluminescence, electron microscopy, and Raman spectroscopy of experimentally shockmetamorphosed zircon. Earth Planet Sci. Lett.* **2002**, *202*, 495–509.
29. Stefaniak, E. A.; Worobiec, A.; Potgieter-Vermaak, S.; Alsecz, A.; Török, S.; Van Grieken, R. Molecular and elemental characterisation of mineral particles by means of parallel micro-Raman spectrometry and scanning electron microscopy/energy dispersive X-ray analysis. *Spectrochim. Acta B* **2006**, *61*, 824.
30. Brenan, C. J. H.; Hunter, I. W. Noninvasive confocal Raman imaging of immiscible liquids in a porous medium. *Anal. Chem.* **1997**, *69*, 45–50.
31. Feofanov, A.; Sharonov, S.; Valisa, P.; da Silva, E.; Naviev, I.; Manfait, M. A new confocal stigmatic spectrometer for micro-Raman and microfluorescence spectral imaging analysis: Design and applications. *Rev. Sci. Instrum.* **1995**, *66*, 3146.
32. Sharonov, S.; Nabiev, I.; Chourpa, I.; Feofanov, A.; Valisa, P.; Manfait, M. J. Confocal three-dimensional scanning laser Raman-SERS-fluorescence microprobe. Spectral imaging and high-resolution applications. *Raman Spectrosc.* **1994**, *25*, 699–707.
33. Brenan, C. J. H.; Hunter, I. W. Confocal image properties of a confocal scanning laser visible light FT-Raman microscope. *Appl. Spectrosc.* **1995**, *49*, 971–976.
34. Behrens, H.; Roux, J.; Neuville, D. R.; Siemann, M. Quantification of dissolved H_2O in silicate glasses using confocal micro-Raman spectroscopy. *Chem. Geol.* **2006**, *229*, 96–112.
35. Cherney, D. P.; Bridges, T. E.; Haris, J. M. Optical trapping of unilamellar phospholipid vesicles: Investigation of the effect of optical forces on the lipid membrane shape by confocal-Raman microscopy. *Anal. Chem.* **2004**, *76*, 4920–4928.
36. Bridges, T. E.; Houlne, M. P.; Harris, J. M. Spatially resolved analysis of small particles by confocal Raman microscopy: Depth profilling and optical trapping. *Anal. Chem.* **2004**, *76*, 576–584.
37. Blach, J.-F.; Warenghem, M.; Bormann, D. Probing thick uniaxial birefringent medium in confined geometry: A polarised confocal micro-Raman approach. *Vib. Spectrosc.* **2006**, *41*, 48–58.
38. Koralay, T.; Kadioglu, S.; Kadioglu, Y. K. A new approximation in determination of zonation boundaries of ignimbrite by ground penetrating radar: Keyseri, Central Anatolia, Turkey. *Environ. Geol.* **2007**, *52*, 1387–1397.
39. Timothy, E.; Tour, L. Analysis of rocks using X-ray fluorescence spectrometry. *The Rigaku J.* **1989**, *6*, 3–9.
40. Johnson, D. M.; Hooper, P. R.; Conrey, R. M. *XRF analysis of rocks and minerals for major and trace elements on a single low dilution Li-tetraborate fused bead*. International Centre for Diffraction Data, **1999**; 843–867.
41. Stephens, W. E.; Calder, W. E. Analysis of non-organic elements in plant foliage using polarised X-ray fluorescence spectrometry. *Anal. Chim. Acta* **2004**, *527*, 89–96.
42. Meng, J. F.; Katiyar, R. S.; Zou, G. T.; Wang, X. H. Raman phonon modes and ferroelectric phase transitions in nanocrystalline lead zirconate titanate. *Phys. Stat. Sol. A* **1997**, *164*, 851–862.
43. Trentelman, K.; Stodulski, L.; Pavlosky, M. Characterization of pararealgar and other light-induced transformation products from realgar by Raman microspectroscopy. *Anal. Chem.* **1996**, *68*, 1755–1761.
44. Bonazzi, P.; Menchetti, S.; Pratesi, G.; Muniz-Miranda, M.; Sbrana, G. Light-induced variations in realgar and beta - As_4S_4; X-ray diffraction and Raman studies. *Am. Mineral.* **1996**, *81*, 874–880.